STANFORD/NASA AMES JOINT INSTITUTE FOR SURFACE AND MICROSTRUCTURE RESEARCH
DEPARTMENT OF MATERIALS SCIENCE AND ENGINEERING
STANFORD UNIVERSITY
STANFORD, CA 94305

FABRICATION AND PROPERTIES OF MULTILAYER STRUCTURES

prepared by

W. A. Tiller

November 1981 SU-DMS-81-R-7

Fourth Semiannual Technical Report for Period 1 March 1981 - 31 August 1981

prepared for

ADVANCED RESEARCH PROJECTS AGENCY
1400 Wilson Boulevard
Arlington, VA 22209

Department of MATERIALS SCIENCE AND ENGINEERING
STANFORD UNIVERSITY

SU-DMS-81-R-7

FOURTH
SEMIANNUAL TECHNICAL REPORT
ON
FABRICATION AND PROPERTIES OF
MULTILAYER STRUCTURES

1 March 1981 - 31 August 1981

This research was sponsored by the
Defense Advanced Research Projects
Agency under ARPA Order No. 3706
Contract No. MDA903-79-C-0484
Monitor: ONR Resident Representative

Contractor: Stanford University

Effective Date of Contract: September 1, 1979

Contract Expiration Date: December 31, 1981

Principal Investigator: William A. Tiller

Phone: (415) 497-3901

Stanford/NASA Ames Joint Institute for Surface and Microstructure Research

Department of Materials Science and Engineering

Stanford University, Stanford, CA 94305

SECURITY CLASSIFICATION OF THIS PAGE *(When Data Entered)*

REPORT DOCUMENTATION PAGE

READ INSTRUCTIONS BEFORE COMPLETING FORM

1. REPORT NUMBER: SU-DMS-81-R-7	2. GOVT ACCESSION NO.: AD-A111089
3. RECIPIENT'S CATALOG NUMBER:	
4. TITLE *(and Subtitle)*: FABRICATION AND PROPERTIES OF MULTILAYER STRUCTURES	5. TYPE OF REPORT & PERIOD COVERED: 4th Semmiannual Technical Report (3/1/81 - 8/31/81)
	6. PERFORMING ORG. REPORT NUMBER:
7. AUTHOR(s): W. A. Tiller, T. W. Barbee, Jr. W. Dibble, L. Nagel, A. Savan, K. Seaward, Y. T. Thathachari	8. CONTRACT OR GRANT NUMBER(s): MDA903-79-C-0484
9. PERFORMING ORGANIZATION NAME AND ADDRESS: Stanford/NASA Ames Joint Institute for Surface and Microstructure Research, Department of Materials Science & Engrg., Stanford University, Stanford, CA 94305	10. PROGRAM ELEMENT, PROJECT, TASK AREA & WORK UNIT NUMBERS:
11. CONTROLLING OFFICE NAME AND ADDRESS: Advanced Research Projects Agency (ARPA) 1400 Wilson Boulevard Arlington, VA 22209	12. REPORT DATE: November 1981
	13. NUMBER OF PAGES:
14. MONITORING AGENCY NAME & ADDRESS *(if different from Controlling Office)*:	15. SECURITY CLASS. *(of this report)*: Unclassified
	15a. DECLASSIFICATION/DOWNGRADING SCHEDULE:

16. DISTRIBUTION STATEMENT *(of this Report)*

Unlimited Distribution

17. DISTRIBUTION STATEMENT *(of the abstract entered in Block 20, if different from Report)*

18. SUPPLEMENTARY NOTES

This contract is awarded under Basic Agreement N00014-79-H-0029, dated 81 September 79, amended by modification P00001 and P00002, issued by the office of Naval Research. This research is sponsored by Defense Advanced Research Projects Agency (DARPA).

19. KEY WORDS *(Continue on reverse side if necessary and identify by block number)*

REACTIVE SPUTTERING, FILM FORMATION, SILICON DIOXIDE, SILICON CARBIDE, SEMICONDUCTOR PROCESSING, THERMAL OXIDATION, INTERSTITIAL SPECIES, CRYSTALLOGRAPHY, MOLECULAR ORBITALS, AMORPHOUS FILMS, INTEGRATED CIRCUITS

→ The goal of this program is to develop

20. ABSTRACT *(Continue on reverse side if necessary and identify by block number)*

This program has as its goal the development of vapor deposition processes for application to integrated circuit technology, (particularly multilayer applications.) Its purpose is to investigate vapor deposition techniques that offer potential for synthesis of materials having new, unique structures and/or of higher quality than currently attainable. Technological application of these materials will be a significant

(over)

DD FORM 1 JAN 73 1473 EDITION OF 1 NOV 65 IS OBSOLETE

UNCLASSIFIED

SECURITY CLASSIFICATION OF THIS PAGE *(When Data Entered)*

consideration in the selection of specific systems for study, particularly multilayer integrated circuit applications.

In this period, an in-situ argon ion-gun cleaning technique has been used to strip the native SiO_2 film from the Si substrates prior to the actual deposition of $Si_{(x)}$ and SiC films. Etch rate data for the native oxide on SiO_2 and the relative film thickness for reactively sputtered SiO_2 films as a function of substrate temperature for etched substrates has been gathered. The relative deposition rate and film texture for single-source sputtered SiC films as a function of substrate type, orientation and film texture was obtained. Exploratory films of SiO_x, WO_x and $NbC_{0.88}$ have been fabricated using the sequential deposition of atomic layers technique.

In the theoretical area, the CNDO/2 technique has been used to determine the energies of formation for bridging oxygen vacancies, V_O, and Frenkel defects, $V_O + O_I$, for a pair of silica structural units (dimer and tetramer ring). In addition, calculations have been made for the adsorption of different molecular chemical species (in the parallel configuration) at the bridging oxygen site of a silica dimer. In the crystallographic modeling of silica structures, energetic calculations have indicated that the O-O distance provides an important restrictive criterion for the configurational changes of the SiO_4 tetrahedra in vitreous silica. Using this criterion as a selective sieve, allowed bridge bond angles for the trimer unit were determined for a pool of 1200 randomly selected examples. Only 61 examples passed the sieve test and these had a distribution of bridge bond angles centered at ~ 145° with a half width of ~30°.

INTRODUCTION

During this fourth six-month period of the program, attention was given to stripping the native oxide from the Si substrates prior to SiO_x and SiC deposition. The SiC deposition was from a single source and a beginning excursion was made into the use of the layer by layer method of film formation for two oxides. The theoretical emphasis continued to focus on both the structural and the energetic aspects of SiO_x. Consideration of the trimer unit appears to be the key needed for understanding vitreous SiO_2 formation on a macroscale. On a microscale, insights into bridging oxygen vacancy, V_O, and Frenkel defect, V_O+O_I, formation energetics have been gathered. To investigate the electrical properties of these films, attention has been given to the development of a new data acquisition system based upon the ac electrical conductance method.

A. Experimental Results

1. Synthesis of SiO_x

Thus far in this program, synthesis experiments via reactive sputtering have consisted of continuous process experiments, i.e., both O_2 and Si were incident on nominally room temperature substrates concurrently with reaction taking place to form SiO_x films. The basic result of this work is that films of uniform composition can be deposited with control of stoichiometry in the range of $0.3 < x \leq 2$. During a given synthesis run, the substrate temperature did not float higher than 50°C.

During the recent period, work was performed to extend and refine these experiments so as to increase our understanding of the process and

of the types of materials which can be synthesized. Two different approaches were taken to the film deposition, the first following directly on the earlier work. In the first approach, the system was improved by adding an in-situ cleaning technique using an argon ion-gun for stripping the native SiO_2 film from the substrate prior to the actual deposition of the reactively sputtered SiO_x films. In addition, a new O_2 gas dispersion ring of rectangular shape was developed for processing rectangular substrates. These new components are illustrated in the chamber schematic of Fig. 1. Some ion-etching data is given in Table I where we see that a substantial etching rate occurs for a 2.0 kV anode voltage located 4" from the substrate with a 4 μm argon pressure and that the procedure is very sensitive to both voltage and distance. Deposition experiments on Si(111) substrates, ion etched at 750 V and 2 mA for 40 minutes, were carried out on heated substrates with the film thickness results given in Table II. There is some question concerning the complete removal of the native oxide for these experiments. Using alpha-step and ellipsometry measurements, the relative film thickness was measured for these films and we see from Table II that the film thickness decreases by a factor of 2 between deposition at 25°C and 660°C. We note also that the film stoichiometry becomes increasingly Si-rich as the substrate temperature is increased. This may be the reason why the plot of film thickness vs. 1/T in Fig. 2 does not reveal a linear relationship.

An additional series of experiments was performed wherein the Si and O_2 were not concurrently incident on the substrate. The chamber system was modified so that the substrate was sequentially exposed to Si and to O_2 so that, in principle, a monolayer of amorphous Si was first deposited and then subsequently oxidized by exposure to an O_2 atmosphere for a time

needed to produce a fraction of a monolayer of O_2 and then the entire process repeated many times to produce an SiO_x film. Some experimental data with this method is presented in Table III. More will be said about this general technique in the next section.

2. Synthesis of Compounds by Atomic Layer Growth

Over the past decade, a new technology for the growth of high perfection crystalline materials has been developed. This technique, "Molecular Beam Epitaxy," allows the synthesis of a wide variety of unique structural deposits. It has characteristically been applied to GaAs and to (Ga,Aℓ)As . In this process, an overpressure of As is maintained at the substrate and the growth of the deposit is defined by the arrival rate of Ga and Aℓ . Atomic layer growth is observed and smooth interfaces can be formed which are abrupt on an atomic or near atomic scale.

In our laboratory, a technique using sputtering technology has been developed that allows sequential deposition of atomic species that can be controlled on a monolayer level and which is uniform for many hundreds of layers. In this process, either (1) separate sputter deposition sources are used for each constituent or (2) a separate region is provided for the substrate to be exposed to reactive gases. The samples are mounted on a turntable rotating at a fixed rate controlled to 0.1% and pass beneath sputter sources so that sequentially deposited layers of the various constituents are incident on the substrate. Individual layer thickness is controlled by the rotation of the substrate table and the deposition rates of the various sources used. In the case of a reactive gas, it appears that the partial pressure of the gas over the substrate is the most

important factor and, when coupled with the rate of substrate motion, determines the exposure of the deposition surface.

At this time, exploratory experiments have been performed on the synthesis of SiO_x and WO_x films. It has been clearly demonstrated that large area films of uniform thickness and stoichiometry can be deposited by this technique. In addition, it has been demonstrated that $NbC_{0.88}$ (of the NaCℓ structure) can be synthesized onto room temperature substrates and exhibits the superconducting transition temperature expected for bulk material of this composition.

3. Synthesis of SiC_x Thin Films

In the last report[1] we described our work on two-source deposition of SiC from Si and C targets. This type of deposition necessarily results in a film of varying concentration from C-rich at one end of the substrate to Si-rich at the other. However, we are primarily interested in stoichiometric β-SiC and ways of improving the crystallinity of sputtered SiC films. Thus, we have changed from the two-source to a single source arrangement. By using a disk of pressed α-SiC particles as the target, we are able to sputter deposit stoichiometric β-SiC thin films.

The actual deposition process has been improved by adding an in-situ cleaning technique. The new deposition configuration shown in Fig. 3 includes the SiC source, the argon-ion gun for surface cleaning and a tin source which can be moved to any desired location in the chamber. The top view of the system shows the substrate travel path for a deposition cycle. After pumpdown to about 4×10^{-6} Torr, the substrate heater is slowly ramped to the deposition temperature. The substrate is rotated

under the argon-ion gun and surface sputter cleaning is initiated. It is essential to prepare a clean surface for good SiC epitaxy to occur so the native SiO_2 on the Si substrate must be completely removed. This involves up to 45 minutes of argon-ion bombardment at 2 mA and 750 V, a voltage considered to be low enough to prevent significant surface damage by ion bombardment. Before being loaded into the chamber, the Si substrates were put through the industry standard "RCA" clean treatment. Near the end of the sputtering cycle, the SiC source is activated and the substrate quickly moved under the activated SiC target. The tin source will be placed so that the Sn is co-sputtered onto the substrate surface along with the SiC, but it will be arranged so that the substrate is rotated through the tin just before being located under the SiC target.

Deposition Rate

Not only is a knowledge of the deposition rate important in order to generate samples of a desired thickness but it also can be used to compare alternate deposition techniques. The deposition rate can even give insight into the degree of crystallinity of the deposited film. For the dual source method at 440 W and a substrate temperature of 700°C, the deposition rate was ~ 2 Å/sec . The single-source deposition is almost twice as fast (~ 4 Å/sec) . The following trends have been observed for the deposition rate, D.R.

$$\text{D.R. (Rm T, } A\ell_2O_3) \approx 1.2 \text{ D.R. (elev T, } A\ell_2O_3) ,$$

$$\text{D.R. (Rm T, Si(111 or 100))} \sim \text{D.R. (elev T, Si(111 or 100))},$$

$$\text{D.R. } (Si_{111}) \approx 1.2 \text{ D.R. } (Si_{100}),$$

and

D.R. (Si) $\approx$ 1.4 D.R. ($A\ell_2O_3$) at Rm T ,

D.R. (Si) $\approx$ 2.0 D.R. ($A\ell_2O_3$) at 700°C .

Any temperature or substrate effects might be attributed to differences in film crystallinity. Amorphous films are expected at low temperatures and mismatched substrates, whereas crystalline films are deposited above 600°C and on well matched substrates. The orientation effect indicates the higher compatibility with the (111) substrate and this appears dramatically in the x-ray analysis. The substrate type effect illustrates the much greater affinity of the SiC for Si than for $A\ell_2O_3$ even though there is a smaller disregistry on the $(1\bar{1}02)$ $A\ell_2O_3$ than on the Si substrates. The greatest deposition rate is observed on the substrate surface having the same symmetry as the "natural" or "preferred" orientation of the deposited β-SiC .

X-Ray Diffractometry

Our primary analytical technique to determine the perfection of the sputtered films is X-ray diffractometry. We use a Read camera to evaluate the extent of preferred orientation. As with the dual source samples, a strongly preferred orientation of the single source films was found. Only the (111) β-SiC reflection is seen. A comparison of one deposition (#178), which had a specular surface and gave the strongest X-ray peak, with other depositions is instructive. The data are presented in Table IV. The relative peak heights were derived from X-ray diffraction peak heights accounting for peak broadening (same in all cases) and SiC film thickness. Ignoring the difference in the 3" and 4" variable which is considered to be a second order effect, the data show that deposition on clean (111) Si greatly enhances film crystallinity for the source operated

at 600 W. Read camera photographs showed a greatly enhanced preferred orientation for sample 178. In addition, the sample's edges and surface were featureless under optical and scanning electron microscopy. By comparison, the more typical film surface appears rough and scanning electron microscopy of the dual source samples revealed columnar growth with a grain diameter ~ 100 A .

Electron Microprobe

Figure 4 presents electron microprobe results for three single source samples and one dual source sample. These samples were analyzed sequentially and were referenced to the same SiC microprobe standard, which is a polished piece of α-SiC . The films are β-SiC deposited on SOS quality sapphire at Rm T, 700°C and 820°C. The single source deposition at Rm T and 700°C appear to be stoichiometric SiC and uniform, while the 820°C sample seems to be off-stoichiometry on the C-rich side but fairly uniform in composition across the sample.

Refractive Index and Optical Transmission

Refractive index (R.I.) measu. ements have been made on a Gaertner L117 ellipsometer equipped with a HeNe laser. Films of SiC deposited at 600 W appear to have R.I. ~ 3.2 while films deposited at 200 W have R.I. ~ 2.6 (literature values give R.I. ~ 2.654 - 2.697 for β-SiC) . The R.I. measurements on the 600 W samples are somewhat suspect because the ellipsometer null was quite broad.

We have been hoping to obtain definitive measurements of the band gap by optical transmission. The sample evaluated previously as having ~ 3.0 eV band gap was re-evaluated on another instrument (Beckman DK-2A

Spectrophotometer) and predicted to have a value of 2.5 when one takes account of film thickness, transmission to absorbance conversion and assuming a direct band gap (assumption of an indirect gap gives a very low-value). The literature values vary with recent reports citing $\sim$ 3.4 for β-Si and $\sim$ 3 for α-SiC .

In this measurement technique, we are concerned with substrate scattering since, to date, our optical transmission substrates have been only singly polished sapphire. Doubly polished sapphire has been on order and is expected soon. We hope to obtain better results with these new substrates.

B. Theoretical Results

1. ac Electrical Conductance Measurement Techniques

In the fabrication of single layer or multilayer structures for device applications, ultimate characterization is usually that of electrical properties. However, two primary inhomogeneities that are not effectively discriminated by the present dc measurement techniques are those at the interfaces in the system and those between the electrodes and the sample. Here, ac measurements of the dielectric response of the film/substrate system can be invaluable for detecting, and separating out, various contributions to various polarizations in the system under study. In spite of the vast amount of studies on Si-O and other film systems, the significance of ac conductivity techniques has not been widely appreciated, primarily because of the difficulty in translating frequency-dependent behavior into actual physical mechanisms. This is because the past techniques have been either (1) accurate but slow or (2) fast but inaccurate and because no generalized equivalent

circuit model has existed via which various contributions to the dielectric response spectrum could be assigned to specific circuit parameters.

From our studies in this area, we have devised a system which promises to overcome all of the above limitations. It allows rapid collection, storage and analysis of large amounts of data at the site of the film experiment. The device is called a dielectric response analyzer. It will measure comparative gain and phase angle between input and output sinusoidal stimuli to the system by means of a dual channel recorder. The rapid sampling features of the recorder will extend the upper frequency range to ~5 MHz and the lower limit to $\sim 10^{-3}$ Hz.

In addition to providing a rapid and accurate measuring system for the following areas: (1) Research on (a) annealing rates, (b) photo-stimulation response, (c) voltage bias effects, (d) charge carrier species, (e) diffusion coefficients and (f) electrode effects, plus (2) Quality Control via (a) conductance, (b) capacitance, (c) dielectric constant, (d) interface integrity and (e) microstructure, the new technique will allow us to test the feasibility of non-contacting electrodes (since the dielectric response is usually a measure of resonance rather than of macroscopic current flow). Such a system would allow the possibility of non-invasively monitoring electrical changes in films under a very broad range of environmental conditions.

2. Modeling of Silica Structures

In our last report for this topic[1], our goal was to identify key parameters for describing the spatial structure of the known

polymorphs of silica without explicitly invoking the unit cell dimensions and space groups. Instead, it was in terms of SiO_2 tetrahedra, the angular parameters describing the orientation of adjacent tetrahedra and of closed rings made up of bridging oxygens. Procedures have been developed for building ring structures of different size and shape; i.e., finding the geometrical constraints in the dimer parameters that would lead to closed rings. We have sought additional restrictive criteria on the parameters involved in building ring structures and have focused on the intermolecular potential energy changes associated with changing O-O and Si-O distances. Trends in the energy variation of the resulting structure as a function of the parameters have been studied. Attention has been focused mainly on the coulombic energy contribution to date; however, semi-empirical procedures for including covalent energy changes and repulsive energy changes are also under development.

The major difficulty in this type of quantitative assessment is in finding a theoretical approach that is simple enough to be manageable and yet accurate enough to give meaningful insight to the problem. In the present case, the dilemma of the simple approach is "what is the partitioning of the total energy, E_T, into the ionic part, E_i, and the covalent part, E_c, and what are the proper partial charges to be used in calculating the ionic part?". One such simple approach is given by Sanderson[2] who was very successful in using it to estimate the atomization energy of the polymer $(SiO_2)_N$. He defined blending coefficients T_i (ionic) and T_c (covalent) such that $T_i + T_c = 1$ with a total energy of

$$E_T = T_i E_i + T_c E_c \qquad (1)$$

He also defined partial charges D(Si) = +0.40 and D(O) = -0.20, for Si and O, respectively, and defined T_i as

$$T_i = \frac{1}{2}[D(Si) - D(O)] \tag{2}$$

Assuming an Si-O distance of 1.61 Å, this led to $T_i = 0.3$ and $T_c = 0.7$ with an Si-O single order ionic bond energy of $E_i = 61.9$ kcal per mole (KPM) and a Si-O single order covalent bond energy of 49.3 KPM. This yields an E_T of 111.2 KPM per SiO bond or an atomization energy for the SiO_2 polymer of 444.8 KPM, which is in excellent agreement with the experimental value of 445.8 KPM. This all seems very fine except there is an appreciable body of data pointing to the charge on the oxygen in SiO_2 being ~ -0.5 to -0.8[3,4] .

Focusing our attention solely on the coulomb energy, CE, it is expressed in KPM for an ion pair by

$$CE = \frac{332\ Q_1Q_2}{R_{12}K} \tag{3}$$

where 332 is the conversion factor to KPM if the charges on the ions Q_1 and Q_2 are in electron units, the separation between the ions, R_{12} is in angstrom units and K is the effective dielectric constant. The parameter K just factors in the polarization effect of the macroscopic environment surrounding ion #2 due to the electric field of ion #1. We shall follow this procedure to estimate CE for a variety of silica clusters; (i) an isolated tetrahedron with no bridging oxygens, (ii) an end unit tetrahedron with one bridging oxygen; i.e., an isolated dimer, (iii) an internal tetrahedral unit in a closed ring with two bridging oxygens;

i.e., an isolated ring and (iv) a tetrahedral unit in an extended volume with four bridging oxygens. Since we are comparing isolated species with no macroscopic silica environment, it is reasonable to set $K = 1$. This will give us the relative coulomb energy for a tetrahedron in all possible structural configurations for the silica network. We can ensure charge neutrality and stoichiometry of the SiO_2 provided we assume a weighting of 1 for all Si, a weighting of 1 for all bridging O and a weighting of 1/2 for all non-bridging O.

In the calculation to follow, we assume a regular tetrahedron (TET) of O with a Si interstitial and an Si-O distance of 1.60 Å which yields an O-O distance of 2.16 Å. We assume a negative charge on the oxygen in electron units of Q_2 and a positive charge on the Si of $+ 2Q_2$. We find the total CE of the unit to be given by

$$CE = 332Q^2 \left\{ 2 \sum_{SiO} \beta + 4 \sum_{SiSi} \beta + \sum_{OO} \beta \right\} KPM \qquad (4a)$$

where

$$\beta = WT_1 \cdot WT_2 / R_{12} \qquad (4b)$$

Considering only a single tetrahedron (no interactions with neighbors), we have $CE/Q_2^2 = -639$, -752 and -832 KPM for an isolated unit (no BRO), an end unit (1 BRO) and an internal unit (2 BRO), respectively. The end unit would correspond to a dimer unit while the internal unit would correspond to a ring unit.

We have also carried out calculations for the monomer, dimer, trimer and closed 6-ring in known crystal structures (using actual coordinates

from the literature). Table V lists CE/Q_2^2 for K = 1 and CE for Q_2 = 0.8 and K = 3.5 for these cases. We note from Eq. (3) that CE varies slowly with distance and expect very little variation within the groups. The energy differences between groups are noticeable; i.e. ~ 12.5 Kcal/mole between monomer and dimer or between dimer and closed 6-ring. The energy of the 6-ring can be considered a very good approximation for the energy of the structure as a whole with the CE of the monomer contributing the major portion of this energy. Since the standard heat of formation of SiO_2 from the elements Si and O ~ 205 KPM, we can expect the covalent energy contribution to be ~ 65 KPM with an E_T ~ 70% ionic. If we had reduced Q_2 to 0.7, then E_T ~ 55% ionic. With either of these choices, ΔE_T for the closed 6-ring between the different polymorphs is ~ 2 - 4 KPM which is the experimentally observed range. Thus, we may deduce that the insight provided by these simple calculations is fully valid for our structural assessment and we may begin to consider changes associated with changing the important angles θ, δ_1, and δ_2 in the dimer.

The dimer can be defined in the usual way via θ, δ_1 and δ_2 or via the alternate scheme described in an earlier report[1]. In this alternate but equivalent scheme, three oxygen atoms form the reference plane (the bridge O plus one O from each tetrahedron). This scheme is convenient for describing ring structures in terms of bridging oxygens. The dihedral angles (α_1, α_2) with respect to this reference plane and the angle O-OB-O (ϕ) define the dimer in this scheme. We have calculated the CE for various values of three angular parameters in both schemes. Some of these results are summarized in Table VI. Four diagrams have been presented, one for each of ϕ = 210, 240, 270 and

300°. In the horizontal direction, one of the dihedral angles, α_2, is varied in steps of 30° from 90° to 270°. In the vertical direction, the other dihedral angle, α_1, is varied from 0° to 120°. Any intersection completely defines a dimer $(\phi,\alpha_1\ \alpha_2)$ and we present the following calculated information: (1) the relative CE for that particular dimer configuration, (2) the minimum O-O separation, r_m, between the two tetrahedra in the dimer and (3) the corresponding Si-O-Si angle (θ).

We note in Table VI that the variations in $E = K(CE)/7.81\ Q_2^2$ are generally within $\sim$ 1 KPM and close to the values computed for the dimers in known structure presented in Table V. The shaded areas of Table VI are the important ones for us here. They correspond to relatively larger values of CE, small values of r_m and values of $\theta \gtrsim 130^0$. All these three quantities are strongly correlated! This is because, as the tetrahedra are brought closer together, the O-O distances are decreased and θ decreases. However, because the CE decays only very slowly with distance, ΔCE is quite small. In nature, the separation between oxygens from neighboring tetrahedra are seldom less than 3.0 Å. Even under very high pressure, the smallest O-O distance between adjacent tetrahedra is about 2.84 Å in low quartz. Thus, these shaded areas in Table VI represent dimer states with a very low occurrence probability.

The change in CE due exclusively to interactions between atoms in different tetrahedra, ΔCE, is presented in Table VII for some randomly selected values from the dozens of dimer configurations analyzed according to the $(\theta,\delta_1,\delta_2)$ scheme. Because of the weighting scheme, the monomer contribution in a dimer should be taken as -96.21 KPM (for K = 1) and not -81.85 as given in Table V. Adding the ΔCE = 5.36 (for

K = 1) from Table VII due to interaction in the dimer gives the proper dimer CE (for K = 1) of -90.85, which is in close agreement with the values given for dimers in known structures (Table V). Once again the correlation is unmistakable between the high positive values of ΔCE and the low O-O distances. Very low values of O-O would mean the intersection of tetrahedra (tetrahedra deformation required). It is also noted that, in general, a $\Delta CE > 6.00$ for (K = 1) corresponds to $\theta \lesssim 120^0$ while a $\Delta CE < 5.00$ for (K = 1) corresponds to $\theta \gtrsim 160^0$. Although it seems as if large $\theta = (\theta \sim 180^0)$ are energetically favorable for the dimer, when the second neighbor interactions are considered (as in a trimer) the energetically favored angles revert to the range of $\theta \sim 144^0$. The non-bonding interactions will also contribute to this feature-favoring a closer packed structure as long as the separations between atoms in the nearby tetrahedra are not less than the van der Waals separation.

Three Membered and Four Membered Rings

The 3-ring of oxygen can be taken to be an equilateral triangle ($\phi = 60^0$). Intuitively, we expect the Si to be outside the triangle so that the tetrahedra do not intersect. Taking the Si of one tetrahedron to lie in the plane of the O-ring, a few combinations of the dihedral angles for the other two tetrahedra were investigated and, for $r_m \gtrsim 3.0$, $\theta \sim 125^0 - 131^0$ generally but with some spread down to $\theta \sim 110^0$. For the 4-ring, we assume it to be square and with the Si of one tetrahedron lying in the plane of the ring. The remaining three tetrahedra are defined by the angular parameters. For the four sets of chosen parameters given in Table VIII, we note only a small variation in CE and

in r_m while $120^0 < \theta < 151^0$. From this we can deduce that a given n-ring will exhibit a spectral distribution of θ peaking at a maximum probability of occurrence for a minimum E_T.

A more detailed account of the study of trimers will illustrate our approach to modeling of silica much better. A trimer will be more indicative of the ring structure that is likely to develop. Three silicons, Si_1, Si_2, and Si_3 and ten oxygens 1-10 form the cluster. Oxygens 1 and 2 and the three silicons are assigned a weight = 1 and the remaining oxygen a weight = .5. There are 78 distances in all among the 13 atoms of the cluster. Taking the central unit as reference, three angular parameters α,β,γ (Fig. 5) are chosen to define each of the other two units. In other words we define two dimers. These angles are conveniently chosen as the Euler angles. The choice of the angular parameters in each case is decided by the ease of computation and the different sets of parameters can be interpreted in terms of one another. The angles β are the angles between the sides of a potential ring structure.

Systematic tabulation of the energy of the trimer as a function of the six angles defining it is too time consuming, may be difficult to interpret and is unnecessary. Instead we decided to sample the structure over the entire 'space' of the six trimer angles. Random values in the full range 0-360° were assigned for the six trimer angles. Sieves were used so that the full calculation (i.e., determining the 78 distances and finding the CE for the trimer) was done only for those passing through the sieve. For these initial calculations the sieve was: when any O-O separation was found to be less than a chosen minimum, the set of angles were abandoned and a new set of random values chosen and the procedure

repeated. In any case the TOT angles were calculated from Si_1 - Si_2 and Si_1 - Si_3. For the initial studies we chose a minimum separation between oxygens = 2.8 A. We chose this value because no known polymorph of silica had O-O separation less than this value and because of the repulsive energy data, using the Lennard-Jones potential parameters of Table IX, indicate a major energy penalty for O-O distances less than this. This choice of O-O minimum will exclude three and four membered rings. It is easy to recognize that at least one of the 9 distances O (5-7) to O (8-10) should be zero for a 3-ring and about 2.6 A for a 4-ring. We could use a different sieve to isolate these rings in the procedures we have described. In the test runs with O-O min = 2.8 A, we initially tried 1200 sets of trimer angles. Of them only 61 passed the sieve. For these 61 cases all the 78 distances of the cluster were calculated and the CE determined. The calculations were abandoned in the rest of the tries whenever the O-O separation fell below 2.8 A. The distribution of the trimer angles over the 1200 tries was examined and found to be uniformly distributed over 0-360°. The distribution of the TOT angles is shown in Fig. 6. The range of the TOT angles is 0-180°. The TOT angles are found to be practically uniformly distributed over a large range 20-140°. It must be recognized that the TOT angles are functions of the dimer angles and uniform distribution of the dimer angles over the range 0-360° need not necessarily imply uniform distribution of the TOT angles. However, the effect of the filter on the distribution of TOT can be seen clearly. The TOT angles for the successful tries are distributed over a much smaller range 110-180 with a peak around 140-150°.

From the calculations on the successful tries, regions corresponding to trimers in known structures can be identified. For instance, in a quick scan the low quartz trimer was unequivocally identified.

The continuation of this work will take the following course: We can use N.B.E. terms (e.g., Lennard-Jones 6-12 potential) instead of the coarse sieve of minimum O-O separation. Five, 6,7... membered rings can be built using similar procedures. This is not a diffiult task. For each additional unit we need three more angles to be specified. We can use Euler angles as we did for the trimer. The distribution of the 3,4,5,6,7...membered rings can be studied.

Alternately we can increase the pool of trimer angles and select the angles from them to build the rings. This will result in fewer rejections. In other words, this pool will represent an initial coarse filter. From any of the angles in this pool, we can make small variations in the trimer angles and find the energy minima, using optimization techniques. Programs have been developed by us for these studies while working on a different molecular simulation problem. Modification of the ring structure, e.g., introduction of new species (vacancies or interstitials) is possible. This initial work, in short, demonstrates that we can do modeling studies on silica and its modifications using relatively simple calculations and providing useful information on the energetics of formation.

3. Energetic Aspects of Varied Atomic and Molecular Species in Silica

One important goal of using a molecular orbital approach to model the energetic aspects of interstitial species in silica is determining

the bridging oxygen vacancy, V_O, and Frenkel defect, $V_O + O_I$, formation energies. This information is essential for modeling the network versus interstitial diffusion for various species as well as for understanding the mechanisms of formation and annealing of fixed oxide charge.

The use and limitations of the CNDO/2 method were discussed in the previous report[1]. The most serious limitation of this MO technique for modeling vacancy formation is that bond lengths tend to be overestimated for second-row elements. CNDO/2 calculations using normal bonding parameters yield equilibrium Si-O distances, d(Si-O) , greater than the values found in natural silicates. For example, the calculated equilibrium Si-O distance using normal bonding parameters and the $H_6Si_2O_7$ cluster is greater than 2.0 Å [3], whereas measured values for silica range from 1.6 to 1.63 Å . Thus, when the bridging oxygen is moved from its normal position in the $H_6Si_2O_7$ cluster, the total energy decreases as d)Si-O(br)) increases. This leads to unreasonably low total energies for a $H_6Si_2O_7$ cluster without a bridging oxygen, V_O .

To decrease the calculated equilibrium values of d(Si-O) , it was necessary to increase the orbital exponent of Si, ξ_{Si} , from the normal value of 1.383[3] to 1.86. Increasing the bonding parameter, ξ_{Si}, contracts the Si orbitals and produces a minimum in the total cluster energy at d(Si-O) = 1.61 for $\xi_{Si} = 1.86$. Although the goal of matching calculated and measured equilibrium d(Si-O) values using CNDO/2 was attained by modifying ξ_{Si} , the electronic structure of the molecule was altered as well. For example, the charge on the bridging oxygen became less negative (from -0.75 to -0.52) indicating an increase in the covalent character of the Si-O bond. High bridging oxygen atomic charges were also found by Newton and Gibbs[4] using ab initio methods to

study $H_6Si_2O_7$ clusters and including d-orbitals in the basis set. No molecular orbital method applied to $H_6Si_2O_7$ appears to simultaneously yield values of atomic charges and bond lengths completely consistent with the experimental values for silica.

With the Si-O bond length-E_T relationship optimized, it was possible to calculate energies of formation of vacancy species. Bridging oxygen vacancy formation in a Si-O network, V_O, is modeled by the following reaction:

$$H_6Si_2O_7 \rightleftarrows H_6S_2O_6V_O + O \; ; \quad \Delta E_T = + 8.967 \text{ eV} . \qquad (5)$$

The $H_6Si_2O_7$ cluster models a O(br) site in an Si-O network whereas $H_6Si_2O_6V_O$ represents the vacancy configuration, V_O. For reaction (5), the equilibrium Si-O bond distance was calculated to be 1.61 A at $\xi_{Si} = 1.86$. An eclipsed dimer configuration similar to that discussed in the previous report was used fixing $< \text{Si-O-Si} = 143.6^0$ and $< \text{Si-O-H} = 180^0$. The vacancy configuration consists of the same dimer configuration without a bridging oxygen. The high positive reaction energy for (5) suggests a low vacancy density would be produced by a reaction involving only neutral species and sites and leading to the release of monatomic oxygen. Performing a similar calculation for the tetramer species using $\xi_{Si} = 1.86$, d(Si-O) = 1.62 and d(O-H) = 0.96 led to $\Delta E_T = + 8.8984$ eV . This is a remarkable correspondence with the results of Eq. (5) considering the differences in d(Si-O) and d(O-H) between the dimer and tetramer.

A much more favorable reaction for the formation of O(br) vacancies is that involving the reaction product O_2; i.e.,

$$2H_6Si_2O_7 \rightleftharpoons 2H_6Si_2O_6V_O + O_2 \; ; \; \Delta E_T = +0.4972 \text{ eV} \qquad (6)$$

where the equilibrium d(O-O) value in O_2 gas is 1.13 A at 0°K. In this case the energy of formation at 0°K for V_O at the free SiO_2 surface is only 0.25 eV. If we assume that $\Delta E_T(T) = \Delta E_T(0^0K)$ and use the equilibrium relationship

$$\Delta E_T(T) = -RT \, \ell n[(X_{V_O}/X_{O(br)})^2 P_{O_2}] = 11.466 \text{ kcal/mole} \qquad (7)$$

We find that about 6% of the bridging oxygen sites at the free surface would be vacant at 1000°K for $P_{O_2} = 1$ atm . Since the energy to form a vacancy in a tetramer was found to be almost identical with that for a dimer and, since in our previous report [1] we found that $\Delta E_T = + 7.387$ eV (Eq. (8)) for placing an O_2 in the center of a tetramer, we expect the following to hold

3 tetramer $\rightleftharpoons$ 2(tetramer-V_O) + (tetramer with O_2 in center); $\Delta E_T \approx +7.884$ eV (8)

so we have for the mole fraction X_{V_O} of bridging oxygen vacancies in the bulk of the tetramer silica

$$X_{V_O} \approx \exp(-60/RT) \qquad (9)$$

with RT in kcals. This would lead to a fraction of about 10^{-13} vacant bridging oxygen sites in the bulk. Since we expect the adsorption energy of an O_2 molecule at the exterior (obtuse angle) of a tetramer to

be much less than in the interior (acute angle) of a tetramer, the actual formation energy for a bridging oxygen vacancy in bulk silica (6-ring rather than 4-ring) will be appreciably smaller than given by Eq. (5).

In Table X, using $\xi = 1.86$, the energy change associated with moving an oxygen from its bridging oxygen site in a tetramer to the center of the ring is given. Thus, for a $V_O + O_I$ in the same ring, the energy of formation is 5.94 eV. However, by using Eq. (4) plus the energy change due to O_2 dissociation in a tetramer; i.e.,

$$\text{tetramer + tetramer with } O_2 \text{ at } (0,0) \rightleftarrows 2(\text{tetramer + O at } (0,0)); \quad \Delta E_T = 4.56 \text{ eV} \tag{10}$$

from our previous report [1] (Eqs. (8) and (9)), the energy for forming a dissociated Frenkel defect in a tetramer solid is given as

$$4 \text{ tetramers} \rightleftarrows 2(\text{tetramers} - V_O) + 2(\text{tetramers} - O_I); \quad \Delta E_T = +3.32 \text{ eV} \tag{11}$$

so that the energy to form a dissociated Frenkel defect is +1.61 eV and this type of dissociated defect is stable in such a tetramer solid.

In the calculations involved with removing a bridging oxygen, its charge changed from ~ -0.5 to -0.2 at 1 Å displacement and to ~ -0.015 at 1.9 Å displacement so that the charge on the removed O and upon the remaining fragment shrink to zero as the O becomes completely separated. The reaction of +2 charged bridging oxygen forming a charged vacancy is much more favorable energetically than Eq. (5); i.e.,

$$H_6Si_2O_7^{2+} \rightleftarrows H_6Si_2O_6V_O^{2+} + O \; ; \quad \Delta E_T = + 0.279 \text{ eV} \qquad (12)$$

However, considering the formation of a +2 charged O(br) site including the electron work function

$$H_6Si_2O_7 \rightleftarrows H_6Si_2O_7^{2+} + 2e^- \; ; \quad \Delta E_T = + 45.586 \text{ eV} \qquad (13)$$

This tells us that Eq. (12) is not favored because the initial charged species is highly unfavored.

Frenkel defect formation energies have also been calculated for both neutral and charged configurations; i.e.,

$$2H_6Si_2O_7 \rightleftarrows H_6Si_2O_6O_I + H_6Si_2O_6V_O \; ; \; \Delta E_T = - 1.065 \text{ eV} \; . \qquad (14)$$

Reaction (14) models the formation of an oxygen interstitial $(H_6Si_2O_8)O_I$ and oxygen vacancy $(H_6Si_2O_6)V_O$ simultaneously from two bridging oxygen sites. The E_T of the oxygen interstitial configuration was calculated using the $H_6Si_2O_7$ configuration as above with an oxygen adatom at an equilibrium distance of 1.25 Å from the bridging oxygen along z ,

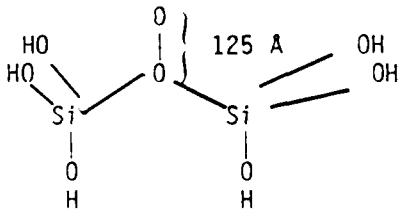

$$H_6Si_2O_8 \equiv H_6Si_2O_7O_I$$

The negative reaction energy of Eq. (14) suggests that the large negative energy of formation of O interstitials more than compensates for the unfavorably positive reaction energy for vacancy formation and that such uncharged Frenkel defects will form spontaneously at the free surface. In the interior of the volume, for 6-rings, the formation of these neutrally charged species is expected to involve a $\Delta E_T > 0$.

For charged Frenkel defects, we have two important possibilities

$$2H_6Si_2O_7 \rightleftharpoons H_6Si_2O_7O_I^{2-} + H_6Si_2O_6V_O^{2+} \; ; \quad \Delta E_T = + 21.75 \text{ eV} \tag{15}$$

and

$$4H_6Si_2O_7 \rightleftharpoons 2H_6Si_2O_7O_I^{2-} + H_6Si_2O_6V_O + H_6Si_2O_6V_O^{2+} + 2e^- \; ; \quad \Delta E_T = + 16.09 \text{ eV} \tag{16}$$

In the case of reaction (16) where two Frenkel defects are formed, the oxygen vacancies of zero charge and +2 charge might be used to model the formation of two vacancies each with a charge of +1 leading to a Frenkel defect formation energy $\sim + 8$ eV for this defect. Clearly, these charged defects do not appear to be energetically favorable and their presence will be enhanced only at the higher temperatures, low P_{O_2} and in the presence of reactions that consume electrons.

Since the E_T of $H_6Si_2O_7$ could be minimized at d(Si-O) = 1.61 by changing the bonding parameter, ξ , the interaction energies determined previously were recalculated to ascertain if any differences in reaction

behavior would result from the new parameterization. It was found that the E_T *vs.* distance relationships for O_2 interactions with O(br) in $H_6Si_2O_7$ are similar for both normal and altered parameterizations. For example, in the configuration with the O-O axis perpendicular to the Si-O-Si plane, the equilibrium O(br)-admolecule distance is 1.15 Å for $\xi = 1.86$ and 1.2 for the normal parameter. However, for the interaction of Si atoms with bridging oxygens, much larger differences were observed in E_T *vs.* equilibrium distance relations between the two parameterizations. For neutral $H_6Si_3O_7$, the equilibrium Si(adatom)-O(br) distance was 1.76 Å for $\xi = 1.86$ but greater than 2.0 Å for the normal parameterization. Likewise d(Si-O(br)) for $H_6Si_3O_7^{2+}$ was 1.58 Å using the new orbital exponent but also greater than 2 Å for the normal value of ξ.

The results of O(br) adatom/admolecule interactions suggest that changing ξ_{Si} will only affect the interaction behavior between O(br) and Si and not between O(br) and other admolecules. This result also confirms the importance of bonding interactions between bridging oxygens and adatoms/admolecules as opposed to interactions between adatoms/admolecules and other atoms such as Si in the $H_6Si_2O_7$ cluster. This conclusion is significant since it supports the validity of CNDO/2 calculations using normal Si bonding parameters for modeling interactions between bridging oxygens and adatoms in aqueous, gas, and crystalline environments.

Further adatom/admolecule - O(br) interaction studies are underway to verify and extend the above results and conclusions. The admolecules include $C\ell_2$, N_2, O_2 H_2 F_2, H_2O and CO_2 using both parameterizations. The results for the normal parameterization ($\xi = 1.383$) are:

$$C\ell_2 + H_6Si_2O_7 \rightleftharpoons H_6Si_2O_7C\ell_2(11); \quad \Delta E_T = -9.509 \text{ kcal/mole} \qquad (17)$$

$$N_2 + H_6Si_2O_7 \rightleftharpoons H_6Si_2O_7N_2(11) ; \quad \Delta E_T = -6.627 \text{ kcal/mole} \qquad (18)$$

$$O_2 + H_6Si_2O_7 \rightleftharpoons H_6Si_2O_7O_2(11) ; \quad \Delta E_T = -2.083 \text{ kcal/mole} \qquad (19)$$

$$H_2 + H_6Si_2O_7 \rightleftharpoons H_6Si_2O_7H_2(11) ; \quad \Delta E_T = -0.603 \text{ kcal/mole} \qquad (20)$$

$$F_2 + H_6Si_2O_7 \rightleftharpoons H_6Si_2O_7F_2(11) ; \quad \Delta E_T = -0.282 \text{ kcal/mole} \qquad (21)$$

The equilibrium distances between the diatomic gas axis and O(br) for the molecules on the right of Eqs. (17)-(24) are, respectively 2.4 Å , 2.1 Å. 2.1 Å, 2.5 Å and 2.7 Å . For contrast, the equilibrium distances in the diatomic gases at θ^0K are d(N-N) = 1.14 Å, d(Cℓ-Cℓ) = 1.98Å, d(O-O) = 1.13 Å, d(H-H) = 0.746 Å and d(F-F) = 1.12 Å. . The minimum energy parallel configuration has the axis of the diatomic molecule parallel to the Si-O-Si plane.

Table XI illustrates the relationship between the silicon-oxygen bridge bond energy, $E_{Si-O(br)}$, and ΔE_T for the reactions 17-21 as well as other admolecule reactions. These results indicate that V_O formation may be favored by reactions with the most negative ΔE_T since the Si-O(br) bond energy increases significanty as ΔE_T decreases.

REFERENCES

1. W. A. Tiller and T. W. Barbee, Jr., "Fabrication and Properties of Multilayer Structures." Third Semiannual Technical Report for Period September 1, 1980 - February 28, 1981, ARPA.
2. R. T. Sanderson, Chemical Bonds and Bond Energy, (Academic Press, 1976), pp 137-138.
3. B. H. W. S. de Jong, "A Spectroscopic and Molecular Orbital Study on the Polymerization of Silicate and Aluminate Tetrahedra in Aluminosilicate Metals, Glasses and Aqueous Solutions," Ph.D. Thesis, Stanford University, December 1980.
4. M. D. Newton and G. V. Gibbs, "Ab Initio Calculated Geometries and Charge Distribution for H_4SiO_4 and $H_6Si_2O_7$ Compared with Experimental Values for Silicates and Siloxanes," Phys. Chem. Minerals 6, 221-246 (1980).
5. B. H. W. S. de Jong and G. E. Brown, Jr., "Polymerization of Silicate and Aluminate Tetrahedra in Glasses, Melts and Aqueous Solutions. II. The Network Modifying Effects of Mg^{2+}, K^+, Na^+, Li^+, H^+, OH^-, F^-, $C\ell^-$, H_2O, CO_2, and H_3O^+ on Silicate Polymers," Geochemica Acta 44, 1627-1642 (1980).

TABLE I

Argon Ion-Etching Data for Oxide Removal from Silicon

Distance (inches)	Voltage (kV)	Argon (μm)	Etch Time (min)	Thickness Change (Å)	Etch Rate (Å/min)
4	0.75	4	30	none	-
4	0.75	8	40	none	-
4	2.0	4	20	245	12.25
4	2.0	4	40	650	16.2
4	2.0	8	20	270	13.5
4	2.0	8	40	580	14.5
5	0.75	4	20	none	-
5	0.75	4	30	none	-
5	0.75	4	40	none	-
5	0.75	8	20	none	-
5	0.75	8	40	none	-
5	2.0	7.5	15	none	-
5	2.0	7.5	20	none	-
5	2.0	7.25	40	130	3.25

TABLE II

Data on Reactively Sputtered SiO_2 Films (Ion etched substrate) - Substrate Temperature Dependence

Run	Temp (°C)	$(Temp)^{-1}$ $(°K)^{-1}$	Film Thickness Alpha-Step (Å)	Film Thickness Ellipsometer (Å)	Refractive Index	Microprobe Analysis O (At %)	Microprobe Analysis Si (At %)
81-215	25	3.3×10^{-3}	6500	7100	1.47	65.57	34.43
81-29	25	3.36	7300	7100	1.46	65.64	34.36
81-216	240	1.95	7000	6550	1.50	63.37	36.63
81-117	340	1.63	5200	4600	1.46	60.13	39.87
81-218	500	1.29	3400	3500	1.53	55.43	44.57
81-220	660	1.07	2500		(1.45)	57.59	42.41
81-221	660	1.07	3300	4500	1.45	47.03	52.97

Conditions: Si(111) substrates; 3" Si source at 4" distance; 500 W rf power for 20 min; P_{Ar} = 4.0 μm; P_{O_2} = 0.30 ± 0.15 μm; Ar ion etching at 750 V, 2 mA for 40 min.

TABLE III

Conditions for Layer-by-Layer Synthesis of SiO_x

Run	Si Source (3" Diam)			Gas Conditions		Rotation Rate (RPM)	# of Layers
	Distance (Inches)	Power Watts	Voltage Volts	Ar	O_2 (μm)		
81-079	5	600	1245	5×10^{-3}	0.47	30	600
81-083	3	700	1350	4×10^{-3}	0.40	115	3461
81-084	3	700	1364	4×10^{-3}	0.29	5.2	156
81-085	3	700	1520	4×10^{-3}	0.25	0.17	176.5

TABLE IV

Relative X-ray Peak Height Data for Various SiC Films

Film#	Film/Substrate	Process[†]	Relative X-ray Peak Height
177	SiC/(100)Si	600W, 720°C, 3"	1.0
178	SiC/(111)Si	600W, 660°C, 4"	5.3
180	SiC/tyco[*]	600W, 660°C, 4"	0.84
184	SiC/(111)Si	200W, 700°C, 4"	1.0
210	SiC/(100)Si	600W, 25°C, 4"	0.0

[*] Tyco ribbon sapphire

[†] SiC Source power, substrate temperature, source-substrate distance

TABLE V

Coulomb Energy for Structural Elements

in Different SiO_2 Polymorphs

Element	CE/Q_2^2 (KPM) (K = 1)	CE(KPM) (K = 3.5) Q_2=0.8
1. Monomer		
Regular Tet	-639.5	-117.05
Low Quartz (10^5PA)	-626.6	-115.72
" " (68 PA)	-633.8	-116.00
" Crystobalite (28°C)	-636.5	-116.50
" " (230°C)	-639.5	-117.05
High " (300°C)	-634.5	-116.14
" " (1200°C)	-636.3	-116.47
2. Dimer		
Low Quartz (10^5 PA)	-701.3	-128.36
" " (68 PA)	-701.2	-128.34
" Crystobalite (28°C)	-707.0	-129.40
High " (300°C)	-704.8	-129.00
3. Trimer		
Low Quartz (68 PA)	-723.7	-132.46
4. Closed 6-Ring		
Low Quartz (10^5 PA)	-769.7	-140.88
" " (68 PA)	-769.2	-140.80
Low Crystobalite (28°C)	-776.6	-142.16
" " (230°C)	-781.0	-142.96
High " (300°C)	-774.5	-141.77
" " (1200°C)	-776.0	-142.04

TABLE VI

Relative Dimer Coulomb Energy (E = KCE/7.81 Q_2^2 KPM)

ϕ=210°	E	-90.82	-90.78	-90.71	-90.68	-90.71	-90.78	-90.82
α_1 = 0	r_m	3.42	3.56	3.44	3.48	3.44	3.56	3.42
	θ	144	142	140	140	140	142	144
	E	-89.69	-89.90	-90.38	-90.78	-91.03	-91.16	-91.15
60	r_m	2.42	2.42	2.94	3.56	3.72	4.06	4.01
	θ	114	119	129	142	157	172	167
	E	-88.66	-89.72	-90.40	-90.86	-91.06	-91.00	-90.69
α_1 = 120	r_m	2.02	2.56	2.92	3.57	3.77	3.77	3.33
	θ	100	114	130	147	159	154	138
ϕ=240°	E	-90.67	-90.93	-90.09	-91.14	-91.09	-90.94	-90.67
0	r_m	3.34	3.68	3.82	4.11	3.82	3.68	3.34
	θ	138	150	162	170	162	150	138
	E	-88.99	-89.72	-90.49	-90.93	-91.12	-91.09	-90.83
α_1=60	r_m	1.83	2.06	2.82	3.68	4.02	4.01	3.34
	θ	104	117	132	150	164	162	146
	E	-86.24	-88.52	-89.67	-90.32	-90.53	-90.36	-89.77
120	r_m	1.25	2.36	2.79	2.79	4.24	2.79	2.79
	θ	81	97	114	218	134	129	115
α_2 =		270	240	210	180	150	120	90

TABLE VI (Cont'd)

ϕ=270°								
	E	-89.95	-90.59	-90.95	-91.07	-90.95	-90.59	-89.95
α_1=0	r_m	3.20	3.47	3.70	3.70	3.70	3.47	3.20
	θ	118	135	152	161	150	135	118
	E	-86.79	-88.54	-89.97	-90.59	-90.78	-90.62	-90.04
60	r_m	1.17	1.55	2.52	3.47	3.54	3.54	3.54
	θ	87	103	120	135	142	136	122
	E	-87.68	-88.78	-89.09	-88.76	-87.66	-85.42	-82.01
120	r_m	1.71	1.71	1.71	1.71	1.71	1.71	1.71
	θ	58	76	92	104	109	105	93
ϕ=300°								
	E	-88.28	-89.53	-90.19	-90.39	-90.19	-89.53	-88.28
α_1=0	r_m	2.08	3.05	3.81	4.31	3.81	3.05	2.08
	θ	94	111	125	180	125	111	94
	E	-81.08	-84.82	-88.39	-89.53	-89.86	-89.61	-88.63
60	r_m	.68	.95	2.04	3.05	3.05	3.05	3.04
	θ	65	82	99	111	116	112	99
	E	-83.57	-85.41	-85.84	-85.15	-82.79	-76.18	-55.98
120	r_m	.97	.97	.97	.97	.97	.97	.97
	θ	34	51	66	78	84	83	76
	α_2 =	270	240	210	180	150	120	90

TABLE VII

ΔCE Contributions Due to Interactions

Between Adjacent Tetrahedra

Random Sample	ΔCE (KPM) (for K = 1) $Q_2 = 0.8$	$\frac{K\Delta CE}{Q_2^2}$ (KPM)	$(O-O)_{min}$ (Å)
1	7.93	61.95	1.42
2	6.96	54.38	1.76
3	6.69	52.27	2.31
4	6.14	47.97	2.67
5	5.76	45.0	2.78
6	5.47	42.73	3.02
7	5.36	41.88	3.40
8	5.10	39.84	3.79
9	5.00	39.06	4.33

TABLE VIII

Variation of θ_{min} , r_m and CE for the 4-Ring

Angles (Deg)			CE (for K=1) $Q_2 = 0.8$ (KPM)	$\frac{KCE}{Q_2^2}$ (KPM)	$(O - O)_{min}$ Å	θ_{min} (Deg)
120	60	180	-99.0	-774	3.47	135
150	30	180	-99.9	-780	3.70	151
120	300	150	-99.0	-774	3.47	120
150	330	180	-99.9	-780	3.70	151

TABLE IX

Lennard-Jones Potential for O - O Interaction

$$U = \frac{Ar_o^6}{2r^{12}} - \frac{A}{r^6}; \quad A = 367, \quad r_o = 3.04 \text{ Å}$$

r(A)	U
2.0	+ 29.6
2.5	+ 0.93
3.0	- 0.23
4.0	- 0.08
5.0	- 0.02
6.0	- 0.01

TABLE X

Undissociated Frenkel Defect Calculation (ξ = 1.86)

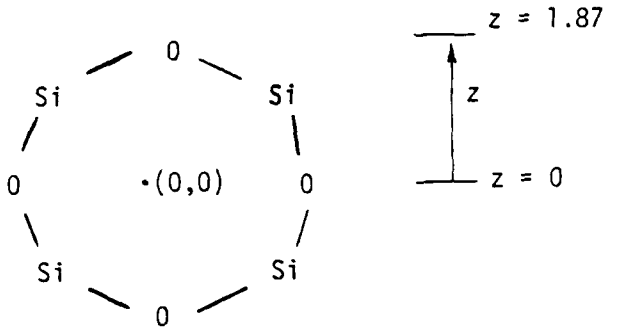

Z	E_T(a.u.)
187	-245.208426
1.7	-245.198887
1.5	-245.192528
1.3	-245.189946
1.0	-245.165820
0.7	-245.090046
0.3	-245.013903
0.0	-244.984417

TABLE XI

Admolecule - Dimer Interaction Energies for Silica

Adspecies	ΔE_T(Kcal/mole)	$E_{Si-O(br)}$(eV)
F_2	-0.3	-17.071
H_2	-0.7	-17.019
O_2	-2.1	-16.565
N_2	-6.6	-16.286
H_2O	-9.0^+	-16.796
$C\ell_2$	-9.5	-16.886
OH^-	-17.0^+	-12.946
$HC\ell$	-28.7	-14.565
$CO_2(I)^*$	-35^+	-14.256
$CO_2(II)^*$	-4.6^+	-12.480
H^+	-317^+	-9.308

*,+ Configuration and energy respectively described in deJong and Brown[5]

FIGURE CAPTIONS

1. (a) Arrangement of deposition source, Ar-cleaner , oxygen supply ring and substrate heater used in the reactive sputtering of SiO_x films.
   (b) Expanded view of the quartz ring for supplying O_2 to the rectangular substrate surface.
2. SiO_x film thickness at constant P_{O_2} as a function of substrate temperature for fixed Si source power.
3. Single-source SiC sputtering system with Ar ion-gun for substrate surface cleaning, and with "portable" tin source situated in most likely position.
4. Electron microprobe results of one dual-source and three single-source SiC depositions showing atomic percentages of Si and C as a function of sample position.
5. (a) Schematic representation of the three tetrahedra involved in a silica trimer (3 Si + 10○).
   (b) Illustration of possible angular variations α, β, γ for the three tetrahedra with one held fixed (6 degrees of freedom).
6. Plot of the number of trimers as a function of bridge-bond angle θ. The upper histogram is for all the choices in the sample (total = 1200); the lower histogram is for the choices passing through the energy sieve $d_{O\text{-}O} \geq 2.8\ A^o$ (total = 61).

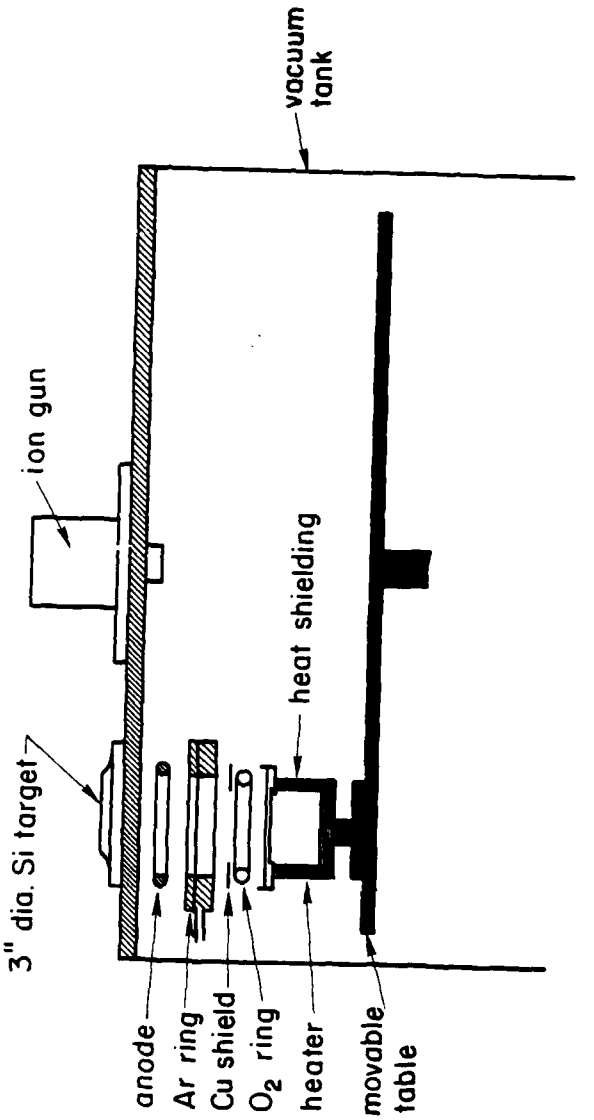
vacuum tank
ion gun
heat shielding
3" dia. Si target
anode
Ar ring
Cu shield
O_2 ring
heater
movable table

FIGURE 1(a)

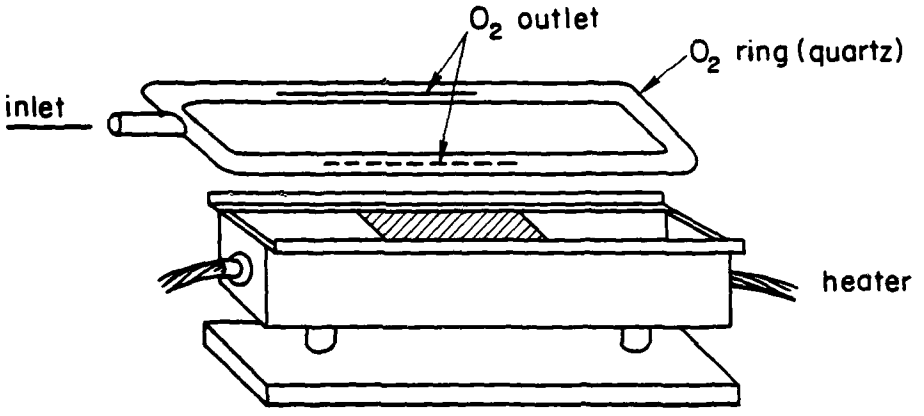

FIGURE 1(b)

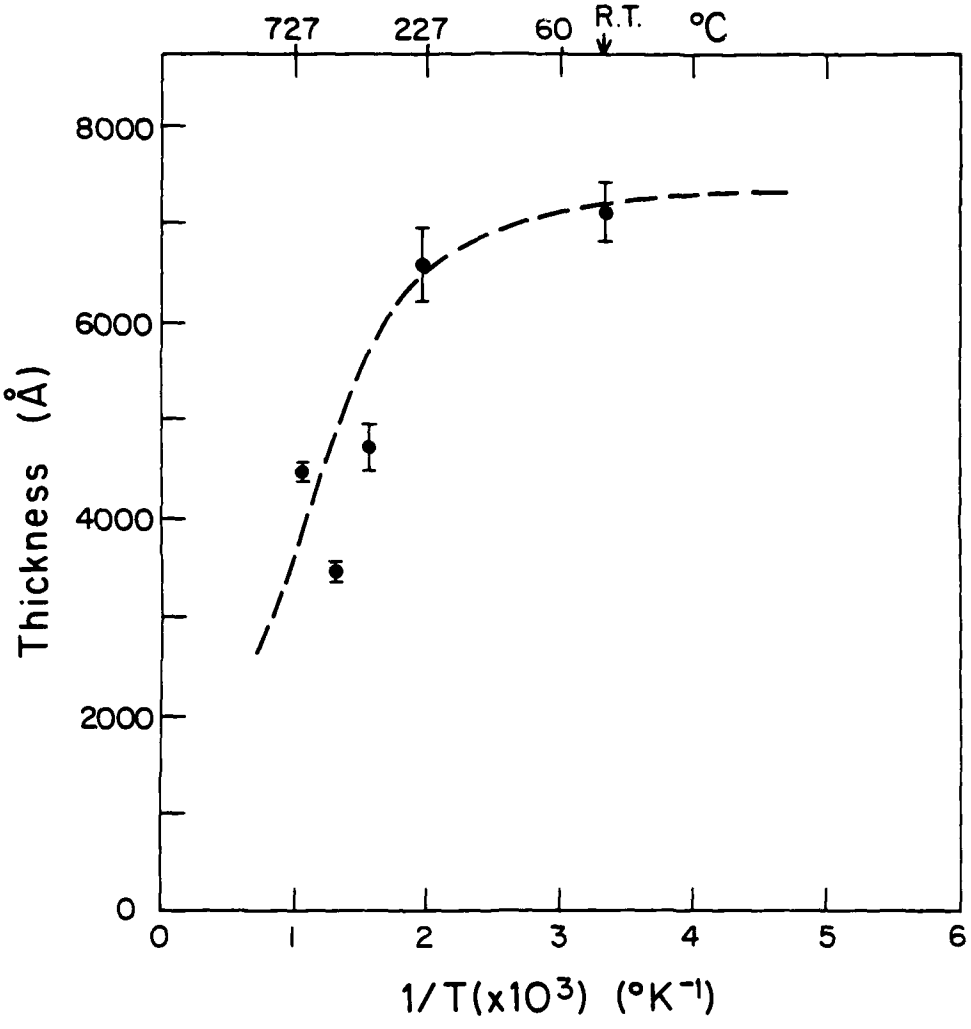
727
227
60
R.T.
°C
8000
6000
4000
2000
0
Thickness (Å)
0
1
2
3
4
5
6
1/T(x10³) (°K⁻¹)

FIGURE 2

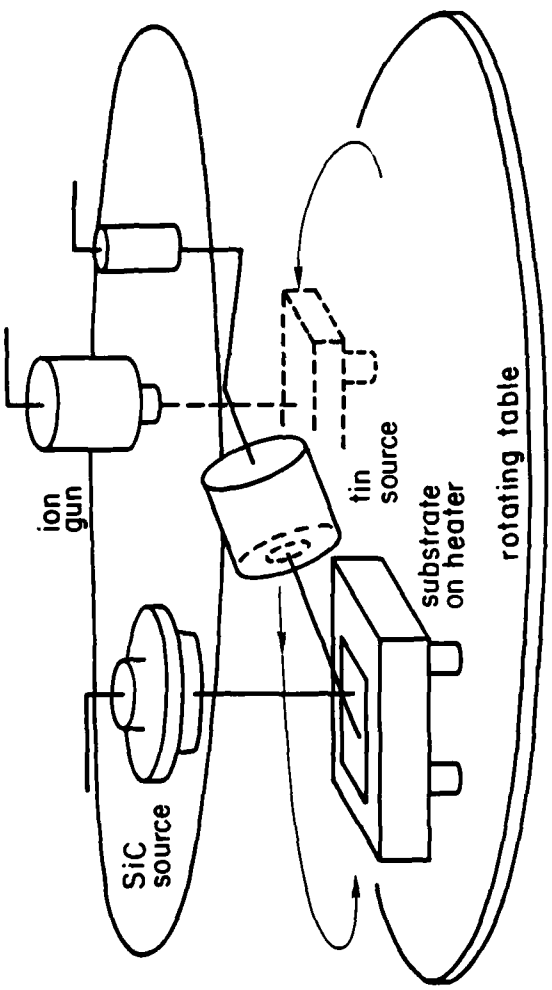
ion gun
tin source
substrate on heater
rotating table
SiC source
SIDE VIEW

FIGURE 3(a)

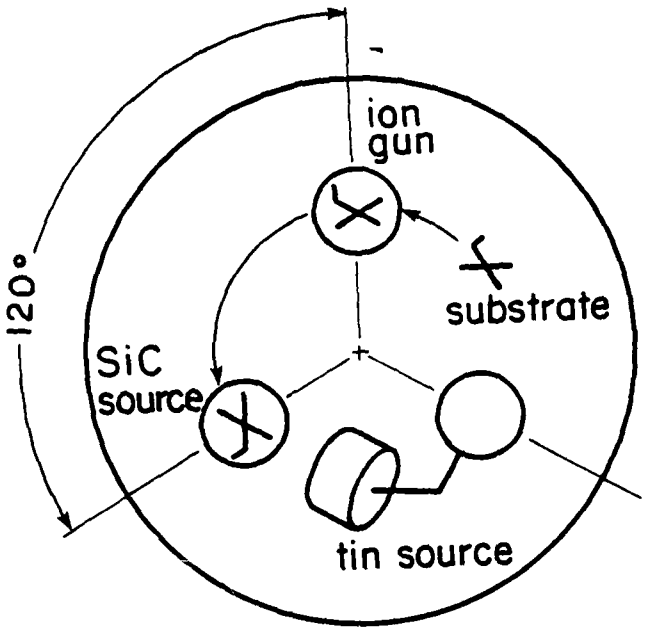

TOP VIEW

FIGURE 3(b)

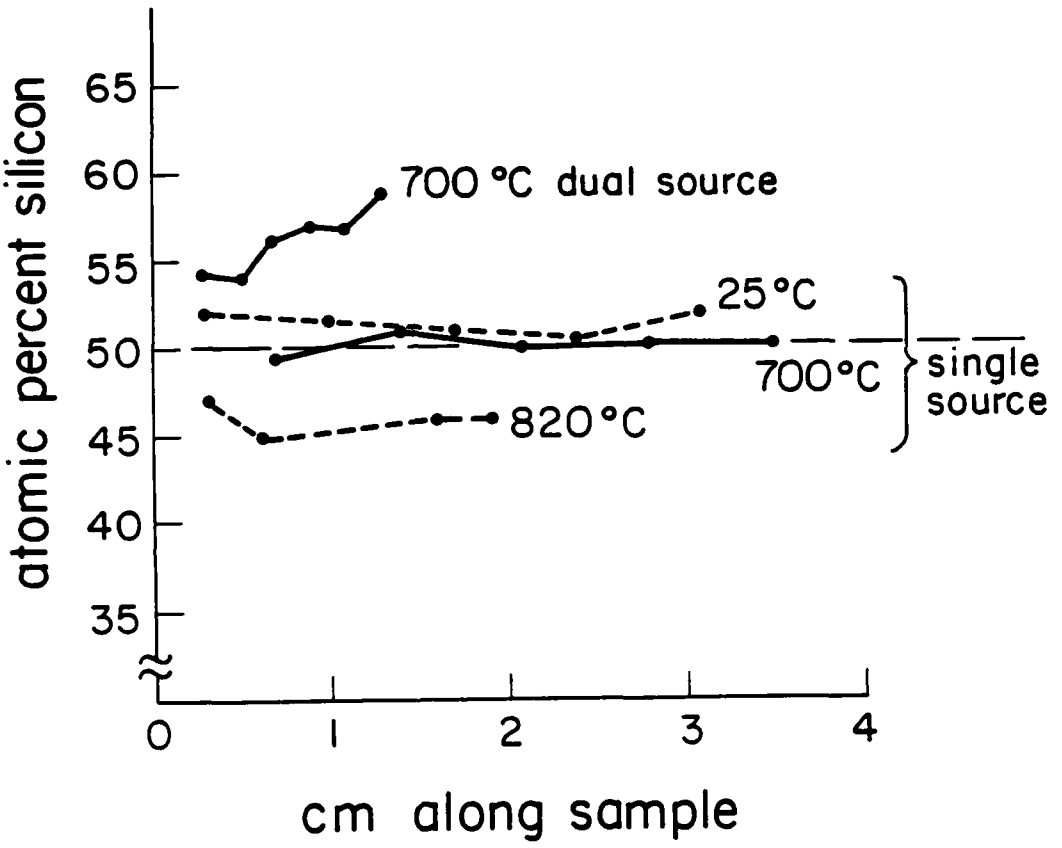
atomic percent silicon
65
60
55
50
45
40
35
700 °C dual source
25°C
700°C
single source
820°C
0
1
2
3
4
cm along sample

FIGURE 4

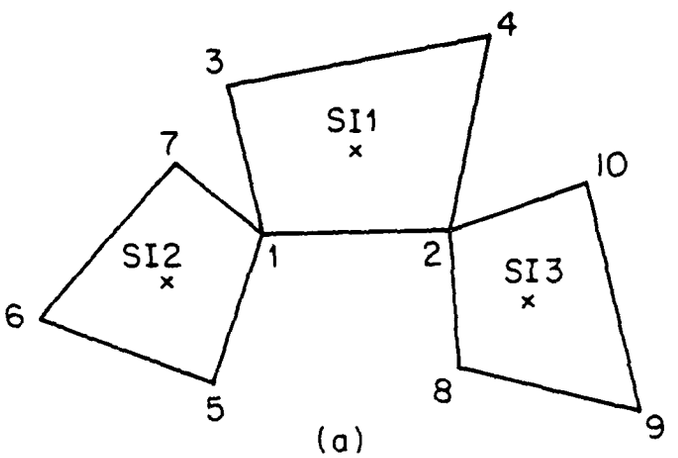
4
3
SI1
7
10
SI2
1
2
SI3
6
5
8
9

(a)

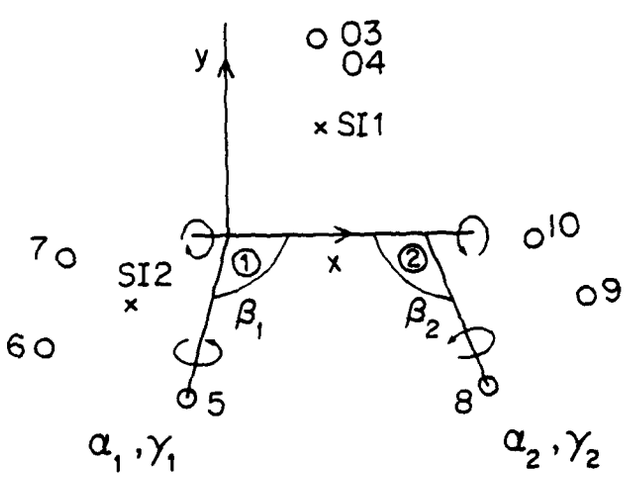
y
03
04
SI1
7
SI2
x
10
09
6
β1
β2
5
8
α1, γ1
α2, γ2

(b)

FIGURE 5

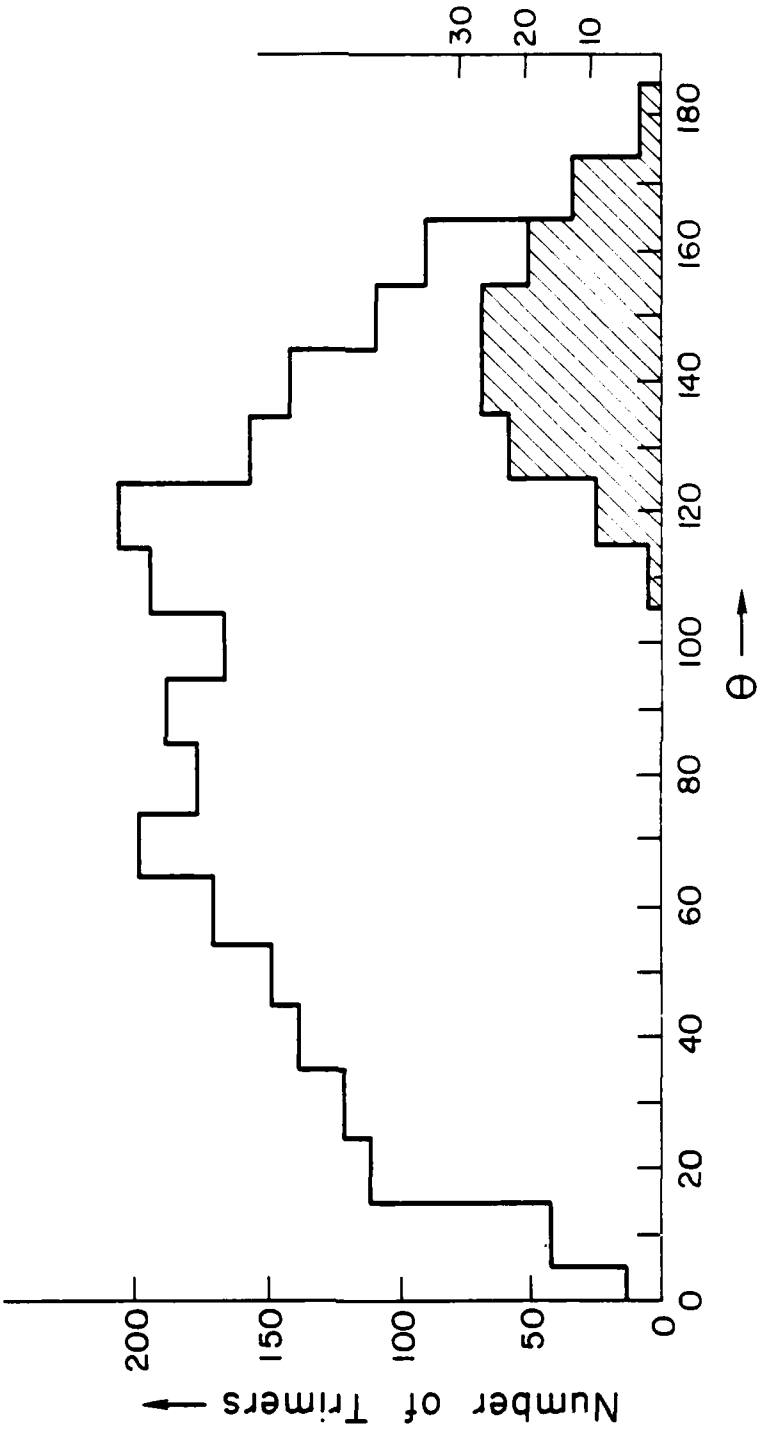
Number of Trimers
200
150
100
50
0
0
20
40
60
80
100
120
140
160
180
θ
30
20
10

FIGURE 6